AIAA JOURNAL
Vol. 44, No. 10, October 2006

Shear Buckling of Flat Orthotropic Stiffened Panels with Application to Glare Material

T. C. Wittenberg,* J. M. A. M. Hol,† and T. J. van Baten‡
Delft University of Technology, 2629 GB Delft, The Netherlands

DOI: 10.2514/1.14970

This paper investigates the shear buckling of flat, stiffened panels of specially orthotropic skin material, for which the stiffeners are assumed to possess both flexural and torsional rigidity. It is shown that the shear buckling behavior can be captured by four generic, nondimensional panel parameters, two of which relate to the skin orthotropy, the other ones representing the flexural and torsional stiffness of the stiffeners. Several design curves, showing the nondimensional shear buckling load as a function of these four panel parameters, are generated using the STAGS FEM code. The validity of the FEM method is demonstrated through comparison with an analytical procedure based on the Rayleigh–Ritz and Lagrangian multiplier methods. Furthermore, to assess the accuracy of the design curves a number of Glare panels containing stiffeners of different shapes and attachment methods typically applied in aerospace structures are analyzed as well. These particular FEM analyses are more realistic than the ones used to generate the design curves in the sense that the exact shape of the stiffeners is modeled and the attachment method is explicitly accounted for. It is shown that the predictions from the design curves are in reasonable agreement with the detailed FEM results.

Nomenclature

A_{ij}	=	in-plane stiffnesses of skin plate, $i = j = 1, 2, 6$
a	=	length of panel
a_{mn}, b_{mn}, c_m, d_m	=	amplitude coefficients in assumed displacement functions
b	=	stiffener spacing
D_{ij}	=	bending stiffnesses of skin plate, $i = j = 1, 2, 6$
EI	=	flexural rigidity of stiffeners
GJ	=	torsional rigidity of stiffeners
i, j, m, n, p, q, M, N	=	integer numbers
K_s	=	shear buckling coefficient
l_m	=	Lagrangian multipliers
P	=	number of stiffeners
q	=	either applied shear flow or integer number, depending on context
t	=	thickness of skin plate
w	=	deflection of skin plate
w_s	=	deflection of stiffeners
x, y	=	coordinates
δ_{ij}	=	1, if $i = j$, =0 otherwise
μ'_F	=	stiffener flexural rigidity parameter
μ'_T	=	stiffener torsional rigidity parameter
ρ'	=	stiffness ratio
φ_s	=	rotation of stiffeners
ψ, θ	=	skin plate orthotropy parameters

Presented as Paper 2054 at the 45th AIAA/ASME/ASCE/AHS/ASC Structures, Structural Dynamics and Materials Conference, Palm Springs, 19–22 April 2004; received 22 December 2004; revision received 9 May 2006; accepted for publication 8 June 2006.

*Stress Engineer, Stork Fokker AESP, Industrieweg 4, 3351 LB Papendrecht, The Netherlands; thomas_wittenberg@sbcglobal.net.

†Associate Professor, Aerospace Structures, Faculty of Aerospace Engineering; j.m.a.m.hol@lr.tudelft.nl.

‡Associate Professor, Aerospace Structures, Faculty of Aerospace Engineering (retired).

I. Introduction

STIFFENED panel assemblies subjected to in-plane shear loading appear frequently in aerospace structures; think, for example, of aeroplane fuselages and wing girders as two obvious examples. With the maturing of lighter and stronger materials, in particular, the fiber-reinforced composites and hybrid materials such as fiber metal laminates (FMLs), it becomes increasingly attractive to use these types of material as a replacement of the traditionally applied aluminum alloys. In the most general sense, infinite combinations of fiber or metal types, layer orientations, and stacking sequences are possible for laminated composites and FMLs, imposing an impractical situation regarding the design process. Therefore, it is desirable to in some way generalize structural analysis where these types of material are involved. This paper deals with such generalized analysis, specifically in relation to the shear buckling behavior of flat, stiffened panels. Moreover, laminated materials are in general not isotropic so that the classical calculation methods for fully metallic panels are no longer applicable.

In conventional shear panel construction it is customary to exploit the shear postbuckling strength for the obvious reason of weight savings. This can only be achieved, however, if the skin of the panel is thin enough, so that initial buckling is characterized by deformations of the individual skin segments bounded by the stiffening members (such as the stringers and frames in a fuselage), which is referred to as *local* buckling. In this case, these stiffening structural elements enforce lines of zero out-of-plane displacements (referred to as *nodes*) and will carry compressive loads, which develop at postcritical loads due to the deficiency of the skin segments to carry compression perpendicular to the buckling waves.

Common design practice for postbuckled shear panels is to treat the individual skin segments as plates with simply supported edge conditions. However, if the skin thickness is relatively great, which will, for example, be the case for future generations of very large airliners, the stiffeners may become too weak to effectively support the skin, resulting in an *overall* buckling mode (where the stiffeners buckle along with the skin). In this case, the initial buckling load calculated by considering the individual plate segments with the assumption of simply supported edges is no longer physically sound, but rather the panel as a whole needs to be considered with the stiffeners explicitly included in the analysis.

When local buckling is in effect, the approach of considering a single skin bay as a simply supported plate is always conservative, because the stiffeners provide at least some torsional restraint to the edges, thereby increasing the plate's buckling resistance. Now, there

are two reasons for including the stiffener torsional rigidity in the buckling analysis to obtain a more accurate estimation of the critical load. The first one is due to the postbuckling strength of a shear panel very often being calculated with (a derivative of) Kuhn's diagonal tension theory [1], which basically consists of a set of empirical formulas that take the ratio of applied shear stress and initial buckling load, the so-called *postbuckling ratio*, as a parameter. If the panel has a considerable amount of postbuckling strength (meaning that it fails at a high postbuckling ratio) the accuracy of the calculated failure load is fairly independent of the accuracy of the initial buckling load estimation because the error is "ratioed out." However, if the failure load is relatively close to the initial buckling load the inaccuracy of the buckling load estimation weighs through into the calculated failure load. The second reason to consider the torsional capability of the stiffeners is that even a small amount of rotational restraint at the plate edges results in a significant increase of the critical load, rendering the simply supported assumption too conservative for efficient design. In other words, a more accurate estimation of the initial buckling load allows for a higher structural efficiency already in the preliminary design stage, which is important considering the ever-increasing performance requirements of aerospace vehicles.

The shear buckling of infinitely long isotropic panels with equally spaced transverse stiffeners was investigated by Stein and Fralich [2] using a Rayleigh–Ritz approach, incorporating Lagrangian multipliers to enforce compatibility of the skin and stiffeners. The deflection of the panel was approximated by a double Fourier series satisfying simply supported conditions at the long edges, and solutions were obtained by separately considering five different buckling modes. In this particular investigation, however, the stiffeners were assumed to possess flexural stiffness only, though, the analysis showed good accuracy with test data. The work of Stein and Fralich was generalized and extended to include the case of clamped edges by Cook and Rockey [3], who presented various design curves relating the nondimensional shear buckling load to two independent nondimensional parameters, being the aspect ratio of the individual plate elements and a quantity expressing the flexural rigidity of the stiffeners relative to the bending stiffness of the skin plate. Comparison with experimental results proved the accuracy of the theoretical results. The Rayleigh–Ritz analysis of [3] was extended to include the torsional rigidity of the stiffeners in [4], rendering the critical buckling load a function of an additional, third, nondimensional panel parameter that represents the ratio of the torsional and flexural rigidity of the stiffeners. In a subsequent paper [5] it was shown that even a small amount of torsional stiffness, such as provided by frequently used open-sectioned stiffeners, gives a buckling load significantly greater than that calculated on the assumption of zero torsional stiffness; this is especially true for high flexural rigidities where the initial buckling mode is a local one.

The buckling of isotropic stiffened panels subjected to pure shear loading was investigated by the authors in [6,7] using the STAGS (structural analysis of general shells) [8] FEM (finite element method) code. The stiffeners in the employed FEM model were represented by beam elements, which allows for the application of independent values for the flexural and torsional rigidities, whereas the skin was modeled with four-node shell elements. It was shown that results presented in [3] could be reproduced [6], demonstrating the validity of the FEM approach. The results including the torsional rigidity of the stiffeners were accurately fitted by appropriate functions of nondimensional panel parameters, which could be conveniently used for design purposes [7]. The main advantage of the finite element method over the semi-analytical methods (such as Rayleigh–Ritz or Galerkin procedures) is its generality, which allows for relatively easy modifications of an existing model if, for example, other boundary conditions and/or a different number of stiffeners needs to be considered, and/or curvature of the panel is desired. When employing the semi-analytical methods, each set of boundary conditions requires its own distinct assumed displacement function, for each of which a rather lengthy algebraic process must be carried out to eventually end up with an eigenvalue problem, which then has to be solved numerically. To obtain the lowest buckling load, it is often required to consider different modes separately, each requiring its own eigenvalue extraction; when using FEM, the critical buckling mode and corresponding load is obtained immediately from one single eigenvalue analysis. The main drawback of the finite element method has traditionally been the expensive computing effort involved, which increases dramatically when the model gets larger. This, combined with the generally better convergence rate of the Rayleigh–Ritz and Galerkin methods, has most often caused the semi-analytical methods to be favored over the finite element method in buckling analysis of shell-type structures. However, with the sheer computing power nowadays available, and with the development of sophisticated, fast solvers such as the VSS vector solver available in STAGS, the computational effort involved with FEM no longer imposes a practical constraint.

One of the earliest studies of the shear buckling of orthotropic plates appears to have been conducted in the late 1920s by Bergmann and Reissner [9], who considered infinitely long, transversely corrugated strips, neglecting the bending stiffness in the longitudinal direction. Partly based on this particular work, Seydel [10,11] derived a solution for the critical shear load of an infinitely long, specially orthotropic plate having simply supported or clamped edges, and for a finite-width plate with all the edges simply supported. The term specially orthotropic refers to the fact that there are no coupling responses such as flexure twist, extension shear, and membrane bending. A more detailed discussion on the buckling of general laminated, anisotropic plates can be found in [12,13]. The buckling of flat, infinitely long anisotropic plates including the case of pure shear loading has been investigated fairly recently by Nemeth [14,15] on the basis of an analytical (Rayleigh–Ritz) approach. Using four nondimensional parameters that essentially capture the plate anisotropy in a general way, Nemeth has produced numerous generic buckling charts which can be conveniently used for design purposes. The nondimensional parameters referred to comprise two "orthotropic" parameters, which pertain to a specially orthotropic plate, and two quantities capturing the flexural anisotropy (i.e., flexure-twist coupling) of the plate.

The present paper investigates the shear buckling behavior of infinitely long, transversely stiffened panels having a specially orthotropic skin. Various results are generated in terms of two orthotropy parameters pertaining to the skin, and two parameters pertaining to the flexural and torsional rigidities of the stiffeners, using a FEM procedure similar to that discussed in [7]. These panel parameters are obtained from the governing buckling partial differential equations by making them nondimensional. To check the validity of the shear buckling loads calculated with FEM, some results are compared to those obtained from an analytical procedure based on the Rayleigh–Ritz method. This analytical procedure is merely an extension of the work by Stein and Fralich [2] to incorporate orthotropic skin material and torsional rigidity of the stiffeners.

Because of the favorable fatigue and weight characteristics over aluminum alloys, the FML Glare, which consists of alternate aluminum sheets and glass fiber prepreg layers, is an excellent candidate material for future generations of very large aircraft [16]. This is particularly demonstrated by Airbus's acceptance of Glare for application in parts of the fuselage of their new A380 aeroplane. To assess the accuracy of the generated design curves, a number of stiffened Glare panels, which fulfil the requirements for special orthotropy, are analyzed with the finite element method. Combinations are investigated of riveted and bonded, open (Z shaped) and closed stiffeners (rectangular section), which are commonly applied in aerospace structures. These FEM analyses are fairly realistic in the sense that the attachment method is accounted for and the exact shape of the stiffeners is modeled.

II. Buckling Analysis

A. Derivation of Nondimensional Design Parameters

The present paper considers a stiffened panel with specially orthotropic skin material having a depth a and stiffener pitch b, and subjected to an in-plane uniform edgewise shear flow q, as illustrated in Fig. 1a. In the analysis, the panel is assumed to be infinitely wide

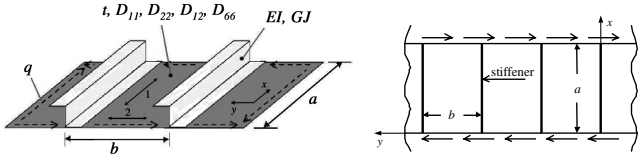

a) b)

Fig. 1 Stiffened panel loaded in shear: a) definition of various design parameters; b) idealization of infinitely wide panel.

(the length of the panel is defined in the stiffener direction so that the individual skin bays have a length a and width b) with the centroids of the stiffeners located at the midsurface of the skin plate, as depicted in Fig. 1b. All the stiffeners are assumed to possess the same flexural and torsional rigidity, EI and GJ, respectively. The bending stiffnesses of the specially orthotropic skin plate are denoted by D_{11}, D_{22}, D_{12}, and D_{66}, whereas, by definition, $D_{16} = D_{26} = 0$.

The total strain energy of the buckled panel per unit wavelength λ in the y direction is composed of the following parts:

1) the bending energy of the skin plate, given by

$$U_p = \frac{1}{2}\int_0^a \int_0^\lambda (D_{11}w_{,xx}^2 + 2D_{12}w_{,xx}w_{,yy} + D_{22}w_{,yy}^2 + 4D_{66}w_{,xy}^2)\,\mathrm{d}x\,\mathrm{d}y \tag{1}$$

2) the flexural energy of the stiffeners, given by

$$U_s^F = \frac{1}{2}\frac{EI}{b}\int_0^a \int_0^\lambda w_{,xx}^2\,\mathrm{d}x\,\mathrm{d}y \tag{2}$$

3) the torsional energy of the stiffeners, given by

$$U_s^T = \frac{1}{2}\frac{GJ}{b}\int_0^a \int_0^\lambda w_{,xy}^2\,\mathrm{d}x\,\mathrm{d}y \tag{3}$$

Furthermore, the work done by the applied loading can be written as

$$\Omega = -q\int_0^a \int_0^\lambda w_{,x}w_{,y}\,\mathrm{d}x\,\mathrm{d}y \tag{4}$$

In Eqs. (1–4) the quantity $w = w(x, y)$ represents the out-of-plane deformation of the panel, and the subscripts denote partial differentiation with respect to the variable(s) following the comma. Now, the total potential energy of the entire system becomes

$$U = U_p + U_s^F + U_s^T - \Omega \tag{5}$$

which may be written as

$$U = \int_0^a \int_0^\lambda F\,\mathrm{d}x\,\mathrm{d}y \tag{6}$$

where

$$F = \frac{1}{2}\left(D_{11}w_{,xx}^2 + 2D_{12}w_{,xx}w_{,yy} + D_{22}w_{,yy}^2 + 4D_{66}w_{,xy}^2 + \frac{EI}{b}w_{,xx}^2 + \frac{GJ}{b}w_{,xy}^2\right) + qw_{,x}w_{,y} \tag{7}$$

Employing variational analysis using Eqs. (6) and (7), the following linearized governing equation for buckling is obtained:

$$D_{11}w_{,xxxx} + 2(D_{12} + 2D_{66})w_{,xxyy} + D_{12}w_{,yyyy} + \frac{EI}{b}w_{,xxxx} + \frac{GJ}{b}w_{,xxyy} - 2qw_{,xy} = 0 \tag{8}$$

Next, the above equation is nondimensionalized by division through the quantity $t\sqrt{D_{11}D_{22}}$, and by introducing

$$\bar{w} = w/t \qquad \bar{x} = x/a \qquad \bar{y} = y/b \tag{9}$$

where t is the thickness of the panel, to yield the expression

$$\frac{1}{\psi^2}\frac{\partial^4\bar{w}}{\partial\bar{x}^4} + 2\theta\frac{\partial^4\bar{w}}{\partial\bar{x}^2\partial\bar{y}^2} + \psi^2\frac{\partial^4\bar{w}}{\partial\bar{y}^4} + \mu_F'\frac{\partial^4\bar{w}}{\partial\bar{x}^4} + \mu_T'\frac{\partial^4\bar{w}}{\partial\bar{x}^2\partial\bar{y}^2} = 2K_s\frac{\partial^2\bar{w}}{\partial\bar{x}\partial\bar{y}} \tag{10}$$

in which

$$\psi = \frac{a}{b}\left(\frac{D_{22}}{D_{11}}\right)^{1/4} \tag{11}$$

$$\theta = \frac{D_{12} + 2D_{66}}{\sqrt{D_{11}D_{22}}} \tag{12}$$

are two parameters reflecting the orthotropy of the skin, and

$$\mu_F' = \left(\frac{b}{a}\right)^2\frac{EI}{b\sqrt{D_{11}D_{22}}} \tag{13}$$

$$\mu_T' = \frac{GJ}{b\sqrt{D_{11}D_{22}}} \tag{14}$$

are two parameters containing information about the relative flexural and torsional stiffness of the stiffeners with respect to the skin bending stiffness, and finally

$$K_s = \frac{qab}{\sqrt{D_{11}D_{22}}} \tag{15}$$

is the nondimensional shear buckling load or coefficient. Consequently, according to Eq. (10), the shear buckling behavior of the panel is completely described by the orthotropy parameters ψ and θ, the flexural stiffness parameter μ_F', and the torsional stiffness parameter μ_T'.

When the contribution of the stiffeners is eliminated from the analysis, Eq. (10) reduces to the governing buckling equation of an unstiffened, specially orthotropic plate. The orthotropy parameters defined by Eqs. (11) and (12) are actually the same as used by Nemeth [14,15], with the small exception that in his work the ψ parameter is defined reciprocally and contains the buckle wavelength λ instead of the plate length a, since plates of infinite length are investigated there. The stiffener parameters μ_F' and μ_T' may be regarded as the orthotropic counterparts of the quantities $\mu_F = EI/Db$ and $\mu_T = GJ/Db$, which were used in [7] for panels with isotropic skin material. Rather than using the stiffener torsional stiffness parameter explicitly, it turns out to be more convenient to introduce a "stiffness ratio" as

$$\rho' = \frac{\mu_T'}{\mu_F'} = \left(\frac{a}{b}\right)^2\frac{GJ}{EI} \tag{16}$$

so that the shear buckling load of the stiffened panel basically becomes a function of the four nondimensional parameters ψ, θ, μ_F', and ρ', and, of course, the boundary conditions at the long edges.

B. Solutions Employing the Finite Element Method

Knowing that the shear buckling load of a specially orthotropic stiffened panel is a function of the four nondimensional parameters defined by Eqs. (11–13) and (16), it is now possible to calculate generic design curves relating K_s, defined by Eq. (15), to these particular parameters. A rather convenient way of generating these curves is by employing the finite element method; in the present investigation the STAGS code [8] is used to analyze the panels. STAGS is a general-purpose FEM program with excellent capabilities for buckling and general nonlinear analysis of shell-type structures.

Because the nondimensional panel parameters cannot be incorporated directly into the FEM model, the properties of the skin plate, stiffeners, and geometry of the panel under consideration

have to be tailored to match the desired values of ψ, θ, μ'_F, and ρ'. The easiest way to tailor the orthotropy parameters ψ and θ in STAGS is to explicitly supply the full **ABD** stiffness matrix of the skin plate. In our case, we will assume certain values for the D_{22} flexural stiffness and the aspect ratio a/b, and denote these by $(D_{22})^0$ and $(a/b)^0$, respectively. Then, from the definition of ψ in Eq. (11), the value of D_{11} follows from

$$D_{11} = \left[\frac{(a/b)^0}{\psi}\right]^4 (D_{22})^0$$

Furthermore, assuming that $D_{12} = D_{66}$, their values follow from the definition of θ in Eq. (12) as

$$D_{12} = D_{66} = \frac{\theta}{3}\sqrt{D_{11}(D_{22})^0}$$

Now that the matrix **D** is completely known (note that $D_{16} = D_{26} = 0$), the elements of the in-plane matrix **A** can be calculated from

$$A_{ij} = 12\frac{D_{ij}}{[(t)^0]^2}$$

where $(t)^0$ is the assumed value for the panel thickness. Although the buckling behavior is governed by the bending stiffness matrix **D**, the **A** matrix is also required by STAGS to calculate the base stress state from which the critical buckling eigenvalue is computed. Note that the matrix **B** is identically zero for a specially orthotropic plate.

To calculate the stiffener properties EI and GJ, one more assumption must be made regarding the stiffener spacing. Defining a value of $(b)^0$ for this particular quantity, the stiffener rigidities become

$$EI = \mu'_F[(a/b)^0]^2(b)^0\sqrt{D_{11}(D_{22})^0} \qquad GJ = \rho'\frac{EI}{[(a/b)^0]^2}$$

which follows from the definitions of μ'_F and ρ in, respectively, Eqs. (13) and (16). At this point, all the design parameters as defined in Fig. 1a (i.e., a, b, t, D_{11}, D_{22}, D_{12}, D_{66}, EI, and GJ) have been given appropriate values that can now be incorporated into the FEM model.

In the previous discussion, certain values were preselected for D_{22}, a/b, b, and t, and the assumption was made that $D_{12} = D_{66}$, from which the rest of the panel quantities were calculated. Because the shear buckling load is a function of the four nondimensional panel parameters only, these four preselected values (as well as the assumption for D_{12} and D_{66}) may, in principle, be chosen arbitrarily. However, to obtain a well-conditioned problem in the FEM buckling analysis, it is preferable to choose practical values so that the numerical eigenvalue extraction process yields realistic results.

The skin of the panel is modeled with the 410-type shell elements available in STAGS. These four-node elements do not include transverse shear deformations, on which assumption the energy formulation of Eq. (1) is based. The stiffeners are represented by the 210-type (Timoshenko-like) beam elements with the centroids located at the midplane of the skin plate, and have a "general" cross section, which means that the values of EI and GJ (actually, I and J only) can be supplied independently. For good performance reasons, the geometry of the individual shell elements is chosen to be square; with this in mind, and recalling that the value of the aspect ratio a/b may be chosen arbitrarily, it follows that the smallest possible FEM model is obtained when the individual skin bays are square, that is, when $(a/b)^0 = 1$. In the present investigation a panel will be considered containing ten stiffeners, dividing it into nine complete skin bays and two half ones at the ends. Although, principally, panels of infinite width (i.e., with an infinite number of stiffeners) are the subject of investigation in this paper, a panel with ten stiffeners may be regarded as the equivalent since it can be shown that a further increase of the number of stiffeners does not substantially affect the shear buckling behavior. Another result of this phenomenon is that the boundary conditions at the short edges of the FEM model have no significant influence as well. In the present analysis, they are taken as simply supported, whereas the long edges can be either simply supported or clamped.

A special computer program was written for the automatic generation of shear buckling results following the procedure described above. For each combination of the parameters ψ, θ, μ'_F, and ρ' an input file is created, which is subsequently passed to STAGS for a linear bifurcation buckling analysis, after which the critical buckling load is read from the output file. This critical load is given in terms of the shear stress resultant or shear flow, so that it has to be nondimensionalized using Eq. (15) to yield the buckling coefficient K_s. This computer program is generic in the sense that the boundary conditions at all four edges and the number of stiffeners in the FEM model can both be changed very easily.

C. Analytical Solution for Simply Supported Edges

To verify the shear buckling loads calculated with the FEM procedure described in the previous section, the problem at hand will be analyzed in an analytical fashion as well. This is done following a Rayleigh–Ritz procedure in conjunction with the Lagrangian multiplier method to account for the contribution of the stiffeners. The approach is essentially an extension of the work of Stein and Fralich [2] to include the torsional rigidity of the stiffeners and orthotropic skin material. Because of the rather lengthy and tedious nature of the analytical process, only the problem is addressed where the long edges of the panel are simply supported. Anyway, the trends found may be expected to be similar for panels with clamped edges. The analytical procedure will be discussed rather concisely in the remainder of this section.

In the application of the Rayleigh–Ritz method a suitable function for the out-of-plane displacement w of the buckled panel must be assumed and substituted into the strain energy expression given by Eq. (5). As discussed in [3], it is only necessary to consider the case where the deflection function has a wavelength of Pb in the y direction, where P is an integer, implying that the buckling deflection is periodic over P stiffeners. A suitable double Fourier series, capable of describing the typically skewed buckling pattern and satisfying simply supported conditions of the skin plate at $x = 0$, a is given by [3]

$$w(x,y) = \sum_{m=1}^{M}\sum_{n=1}^{N} a_{mn}\sin\frac{m\pi x}{a}\sin\frac{2\pi n y}{Pb} + \sum_{m=1}^{M}\sum_{n=0}^{N} b_{mn}\sin\frac{m\pi x}{a}\cos\frac{2\pi n y}{Pb} \tag{17}$$

Substitution of this function into Eq. (1) and performing the necessary integrations (noting that $\lambda \to Pb$) eventually leads to the following expression for the bending strain energy of the skin plate:

$$U_p = \frac{\pi^4\sqrt{D_{11}D_{22}}}{8Pab}\sum_{m=1}^{M}\sum_{n=0}^{N} A_{mn}(a_{mn}^2 + b_{mn}^2)(1+\delta_{0n}) \tag{18}$$

In a similar manner, substitution of Eq. (17) into Eq. (4) yields

$$\Omega = -4\pi q\sum_{m=1}^{M}\sum_{n=0}^{N}\sum_{p=1}^{M} a_{mn}b_{pn}\frac{mnp}{m^2-p^2} \qquad (m \pm p \text{ odd}) \tag{19}$$

for the work done by the applied shear flow q.

For the contribution of the P stiffeners to the total energy of the system, Eqs. (2) and (3) are rewritten as

$$U_s^F = \frac{EI}{2}\sum_{i=1}^{P}\int_0^a (w_s^i)_{,xx}^2\,\mathrm{d}x \tag{20}$$

$$U_s^T = \frac{GJ}{2}\sum_{i=1}^{P}\int_0^a (\varphi_s^i)^2\,\mathrm{d}x \tag{21}$$

where $\varphi_s^i = \varphi_s^i(x)$ represents the rotation of the ith stiffener. The deflection of the ith stiffener, located at $y = (i-1)b$, is assumed to be given by

$$w_s^i(x) = \sum_{m=1}^{M} c_m^i \sin\frac{m\pi x}{a} \tag{22}$$

while for the rotation of the stiffeners the function

$$\varphi_s^i(x) = \sum_{m=0}^{M} d_m^i \cos\frac{m\pi x}{a} \tag{23}$$

is adopted. Substitution of these assumed functions into Eqs. (20) and (21) yields

$$U_s^F = \frac{\pi^4 EI}{4a^3}\sum_{i=1}^{P}\sum_{m=1}^{M}(c_m^i)^2 m^4 \tag{24}$$

$$U_s^T = \frac{aGJ}{4}\sum_{i=1}^{P}\sum_{m=0}^{M}(d_m^i)^2 \tag{25}$$

For the stiffener deformations to be compatible with those of the skin plate, the following conditions must be met:

$$\begin{aligned} w(x, ib) - w_s^i(x) &= 0 \quad (i = 0, 1, \ldots, P-1) \\ w_{,xy}(x, jb) - \varphi_s^j(x) &= 0 \quad (j = 0, 1, \ldots, P-1) \end{aligned} \tag{26}$$

(note the changed summation boundaries and indices) which, upon substitution of Eqs. (17), (22), and (23), leads to

$$\sum_{n=1}^{N} a_{mn}\sin\tfrac{2\pi in}{P} + \sum_{n=0}^{N} b_{mn}\cos\tfrac{2\pi in}{P} - c_m^i = 0 = g_m^i \quad \begin{matrix}(m = 1, 2, \ldots, M)\\ (i = 0, 1, \ldots, P-1)\end{matrix} \tag{27}$$

and

$$\tfrac{2\pi^2 m}{Pab}\left(\sum_{n=1}^{N} a_{mn} n\cos\tfrac{2\pi jn}{P} - \sum_{n=1}^{N} b_{mn} n\sin\tfrac{2\pi jn}{P}\right) - d_m^j = 0 = g_m^j \quad \begin{matrix}(m = 1, 2, \ldots, M)\\ (j = 0, 1, \ldots, P-1)\end{matrix} \tag{28}$$

The application of the Rayleigh–Ritz method implies that the total strain energy of the system must by minimized with respect to the a_{mn} and b_{mn} coefficients for the assumed displacement function in Eq. (17) to represent a buckling mode of the panel. This minimization must be carried out under the conditions given by Eqs. (27) and (28), so that the problem is actually an optimization problem with equality constraints, for which the Lagrangian multiplier method comes into picture. Defining a function $f(a_{mn}, b_{mn}, c_m^i, d_m^j)$ as

$$f(a_{mn}, b_{mn}, c_m^i, d_m^j) = \frac{8Pab}{\pi^4\sqrt{D_{11}D_{22}}}(U_p + U_s^F + U_s^T - \Omega) \tag{29}$$

and introducing the Lagrangian multipliers l_m^i and l_m^j the objective function becomes

$$F(a_{mn}, b_{mn}, c_m^i, d_m^j, l_m^i, l_m^j) = f(a_{mn}, b_{mn}, c_m^i, d_m^j) + \sum_{i=0}^{P-1}\sum_{m=1}^{M} l_m^i g_m^i(a_{mn}, b_{mn}, c_m^i) + \sum_{j=0}^{P-1}\sum_{m=1}^{M} l_m^j g_m^j(a_{mn}, b_{mn}, d_m^j) \tag{30}$$

The conditions for the minimum of this function are

$$\frac{\partial F}{\partial a_{mn}} = \frac{\partial F}{\partial b_{mn}} = \frac{\partial F}{\partial c_m^i} = \frac{\partial F}{\partial d_m^j} = \frac{\partial F}{\partial l_m^i} = \frac{\partial F}{\partial l_m^j} = 0 \tag{31}$$

Substitution of Eqs. (18), (19), (24), (25), (27), and (28) into Eq. (30) and performing the above differentiations leads to, after some algebraic manipulations, the following system of simultaneous equations:

$$\begin{aligned} 2A_{mn}a_{mn} + mS\textstyle\sum_{p=1}^{M} b_{pn}\frac{np}{m^2-p^2} + 2P^2m^4\mu_F'\sum_{q=1}^{N} a_{mq}\Delta_{nq}^{(1)} + 8m^2n\mu_T'\sum_{q=1}^{N} a_{mq}\Delta_{nq}^{(2)} &= 0 \quad (m \pm p \text{ odd}) \\ 2A_{mn}b_{mn}(1+\delta_{0n}) + mS\textstyle\sum_{p=1}^{M} a_{pn}\frac{np}{p^2-m^2} + 2P^2m^4\mu_F'\sum_{q=0}^{N} b_{mq}\Delta_{nq}^{(2)} + 8m^2n\mu_T'\sum_{q=0}^{N} b_{mq}\Delta_{nq}^{(1)} &= 0 \quad (m \pm p \text{ odd}) \end{aligned} \tag{32}$$

where $m = 1, 2, \ldots, M$ and $n = 1, 2, \ldots, N$ for the a_{mn} coefficients, and $m = 1, 2, \ldots, M$ and $n = 0, 1, \ldots, N$ for the b_{mn} coefficients, and

$$A_{mn} = \left(\frac{Pm^2}{\psi}\right)^2 + 8\theta(mn)^2 + \left(\frac{4\psi n^2}{P}\right)^2 \tag{33}$$

$$S = \frac{32Pabq}{\pi^3\sqrt{D_{11}D_{22}}} \tag{34}$$

and

Table 1 Convergence of analytical and FEM buckling loads

Panel parameters				K_s analytical (M, N)[a]			K_s FEM (no. elements)[b]	
ψ	θ	ρ'	$(\mu'_F)^{1/2}$	(4, 8)	(8, 16)	(12, 24)	(20 × 20)	(40 × 40)
0.2	0.0	20.0	15.0	170.4	169.8	169.8	166.8	169.0
0.2	1.0	20.0	15.0	276.5	275.1	275.0	274.2	274.5
0.2	3.0	20.0	15.0	441.1	438.7	438.5	440.2	438.8
1.0	0.0	20.0	15.0	82.2	80.2	79.7	79.3	79.0
1.0	1.0	20.0	15.0	127.6	125.1	124.6	124.6	124.0
1.0	3.0	20.0	15.0	214.3	210.5	209.9	210.7	209.5
5.0	0.0	0.05	3.0	188.5	183.9	183.0	184.8	185.2
5.0	0.0	20.0	15.0	611.8	317.0	307.3	293.1	302.9
5.0	1.0	0.05	3.0	218.2	214.7	214.2	216.3	216.4
5.0	1.0	20.0	15.0	691.0	455.8	453.3	446.0	450.2
5.0	3.0	0.05	3.0	272.8	269.6	269.2	271.0	270.6
5.0	3.0	20.0	15.0	832.4	688.4	685.7	684.5	683.0

[a]Minimum of results for $P = 2$ and $P = 4$. [b]Per skin bay, in both directions; panels with 10 stiffeners.

$$\Delta_{nq}^{(1)} = 0,\ \Delta_{nq}^{(2)} = 0 \quad \text{if } n - q \bmod P \neq 0 \quad \text{and} \quad n + q \bmod P \neq 0$$

$$\Delta_{nq}^{(1)} = 1,\ \Delta_{nq}^{(2)} = 1 \quad \text{if } n - q \bmod P = 0 \quad \text{and} \quad n + q \bmod P \neq 0$$

$$\Delta_{nq}^{(1)} = -1,\ \Delta_{nq}^{(2)} = 1 \quad \text{if } n - q \bmod P \neq 0 \quad \text{and} \quad n + q \bmod P = 0$$

$$\Delta_{nq}^{(1)} = 0,\ \Delta_{nq}^{(2)} = 2 \quad \text{if } n - q \bmod P = 0 \quad \text{and} \quad n + q \bmod P = 0$$

where $a \bmod b = 0$ means that a/b is an integer; if $a \bmod b \neq 0$, a/b is a noninteger. This system may be written symbolically as

$$\mathbf{X}_1\mathbf{y} + S\mathbf{X}_2\mathbf{y} + \mathbf{X}_3\mathbf{y} = \mathbf{0} \tag{35}$$

where $\mathbf{y}$ is a vector containing the a_{mn} and b_{mn} coefficients,

$$\mathbf{y} = \{a_{11}, a_{12}, \ldots, a_{MN}, b_{10}, b_{11}, \ldots, b_{MN}\}^{\mathrm{T}} \tag{36}$$

and $\mathbf{X}_1$, $\mathbf{X}_2$, and $\mathbf{X}_3$ are matrices pertaining to the contributions of the A_{mn} coefficients, the load parameter S, and the stiffener rigidities μ'_F and μ'_T, respectively. Equation (35) can now be rewritten in the form of an eigenvalue problem as

$$-(\mathbf{X}_1 + \mathbf{X}_3)^{-1}\mathbf{X}_2\mathbf{y} = \frac{1}{S}\mathbf{y} \tag{37}$$

where the quantity $1/S$ represents the eigenvalues of the matrix $-(\mathbf{X}_1 + \mathbf{X}_3)^{-1}\mathbf{X}_2$, of which the largest one determines the critical (i.e., lowest) value of S, $S_{\min}$, and thus the buckling load q_{cr}. From the definition of S, the value of the buckling coefficient follows from

$$K_s = \frac{\pi^3 S_{\min}}{32P} \tag{38}$$

In principle this solution is exact, the only limitation being one of computation, in that only a finite number of terms can be taken in the Fourier series. For increasing values of M and N the buckling load converges to the exact solution so that, in practice, a convergence criterion must be defined determining the truncation values of the Fourier series.

III. Buckling Results

A. Comparison of FEM and Analytical Results

For both the FEM and analytical approach, the accuracy of the calculated shear buckling load is strongly dependent on the level of discretization of the problem. In the analytical case, a progressive increase of the values of M and N causes the results to converge to the "exact" solution. For the FEM analysis, this is established by increasing the number of elements, or, rather, the number of nodes. Table 1 presents the results obtained from both approaches for a number of selected combinations of panel parameters, the choice of which will be elaborated on next, and different (increasing) levels of discretization, from which the convergence characteristics can be studied.

Because the shortest buckling wavelengths occur for a local buckling mode and clamped plate edges at the stiffener locations, the level of discretization required for a converged solution is highest for the larger values of the flexural stiffness parameter and stiffness ratio, μ'_F and ρ', respectively. It turns out that for values of $(\mu'_F)^{1/2} = 15$ and $\rho' = 20$ the condition of local buckling and clamped edges at the stiffeners is in effect for all the combinations of ψ and θ investigated. [Note that the quantity $(\mu'_F)^{1/2}$ is used rather than μ'_F because it is more convenient for plotting purposes.] Therefore, as these particular values constitute the drivers for the convergence characteristics of the buckling solution, Table 1 presents results for $(\mu'_F)^{1/2} = 15$ and $\rho' = 20$ for extreme and intermediate values of ψ and θ. For reference, Table 1 also shows the convergence characteristics for panels with $\psi = 5$ and intermediate values of the flexural stiffness parameter and stiffness ratio. The analytical buckling loads were calculated for $P = 2$ and 4 (i.e., two and four stiffeners), the lowest of the two corresponding results being the values listed in Table 1. (Note that the FEM results were obtained for 10 stiffeners, thereby simulating infinitely wide panels.) From Table 1 it can be concluded that the analytical results for $(M, N) = (12, 24)$ are generally equal to those obtained with STAGS using a mesh of 40×40 shell elements for the individual skin bays. Furthermore, convergence of the analytical solutions is demonstrated by the small difference in buckling loads calculated with the (12, 24) and (8, 12) series approximations. The same can be said for the FEM results with a 40×40 and 20×20 mesh, from which it can be concluded that a 20×20 mesh is generally a sufficient enough discretization to obtain an accurate solution. The correlation of the analytical and FEM results is clearly eminent from Table 1. The poorest convergence characteristics are generally seen for the more extreme values of orthotropic parameters ψ and θ.

It is interesting to see that some of the FEM results converge from below, whereas the analytical buckling loads all converge from above. To get an idea whether these convergence phenomena are characteristic to FEM solutions in general, or particular to the STAGS code (more specifically, element formulation, eigenvalue extraction technique, etc.) presently used, the panel configurations in question were analyzed with MSC NASTRAN as well. From the results presented in Table 2 it shows that the NASTRAN solutions, like the analytical ones, converge from above for all six panel configurations investigated. The associated buckling modes from both NASTRAN and STAGS are depicted in Fig. 2, and they are seen to be similar in general. The STAGS buckling modes appear to be a little "irregular" though, especially for the 20×20 meshes. We will not go out of our way to seek a detailed explanation for the different

Table 2 Comparison of buckling loads from STAGS and NASTRAN for selected panel configurations

Panel parameters				K_s STAGS (no. elements)[a]		K_s NASTRAN (no. elements)[a]	
ψ	θ	ρ'	$(\mu'_F)^{1/2}$	(20 × 20)	(40 × 40)	(20 × 20)	(40 × 40)
0.2	0.0	20.0	15.0	166.8	169.0	178.0	167.5
0.2	1.0	20.0	15.0	274.2	274.5	276.3	274.5
5.0	0.0	0.05	3.0	184.8	185.2	187.2	185.6
5.0	0.0	20.0	15.0	293.1	302.9	336.7	313.6
5.0	1.0	0.05	3.0	216.3	216.4	217.0	313.2
5.0	1.0	20.0	15.0	446.0	450.2	463.4	451.8

[a]Per skin bay, in both directions; panels with 10 stiffeners.

convergence characteristics of some of the STAGS buckling loads, but leave this subject with the remark that things such as the formulation of the elements and the eigenvalue extraction technique play a role herein.

From the buckling mode plots it can also be deduced that the parameter ψ could be considered an "effective" aspect ratio of the individual, local bay plates, where large values represent a long plate and low values represent a wide plate. This also explains why the results converge at a slower rate for high and low values of ψ; the buckling pattern consists of multiple half-waves (of which the direction depends on whether ψ is greater or less than zero, but with increasing numbers for either increasing or decreasing values of ψ) and hence a higher level of descretization is required to accurately represent the buckling mode.

B. Design Curves

A number of design charts relating the shear buckling coefficient K_s to a range of nondimensional panel parameters are presented in Fig. 3. These results were calculated using the FEM approach discussed in Sec. II.B with a 20 × 20 mesh for the individual skin bays and ten stiffeners simulating an "infinitely" wide panel. Solutions are given for panels with the long edges either simply supported or clamped. Because only a limited range of parameters can be plotted effectively, practical values were selected for the skin plate orthotropy parameters ψ and θ.

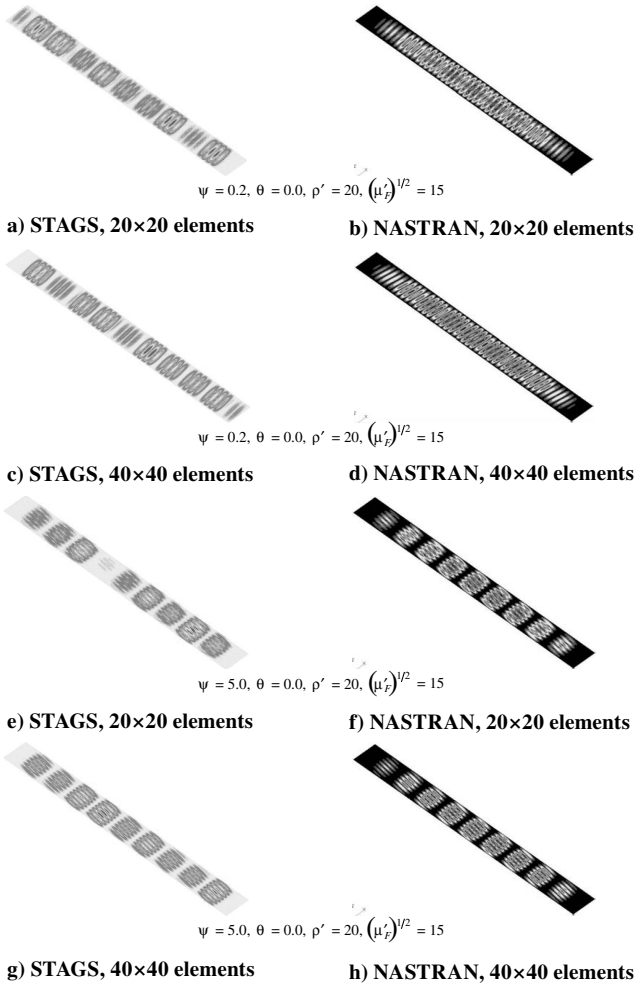

Fig. 2 Comparison of buckling modes obtained with STAGS and NASTRAN for selected panel configurations listed in Table 2.

Characteristic for all curves in Fig. 3 is that the shear buckling load increases with increasing flexural stiffness parameter μ'_F for all values of the stiffness ratio ρ'. For all cases where the stiffeners have no torsional rigidity (i.e., $\rho' = 0$), K_s increases up to a certain "critical" value, beyond which the buckling load is more or less constant and thus independent of μ'_F. The physical explanation of this phenomenon is that the flexural stiffness of the stiffeners contribute to the overall bending stiffness of the plate (think of a "smearing" effect), until they are rigid enough to enforce local "plate" buckling of the individual skin bays. The edges of these skin bays are almost simply supported at the stiffener locations in this case; there is a small rotational stiffness at a nodal line provided by the adjacent bay resulting from "incompatibility" of the shear buckling deformations. Once this condition is reached, and, thus, the stiffeners are already enforcing nodes in the buckling pattern, a further increase of flexural stiffness has no effect.

For values of $\rho' > 0$ the actual value of the rotational stiffness of the stiffeners (μ'_T and, implicitly, GJ) increases with μ'_F due to the definition of the stiffness ratio given in Eq. (16). This means that, when local buckling is in effect, the value of the buckling load can still increase with increasing μ'_F until the fully clamped condition is reached, after which a further increase of GJ of the stiffeners has no effect. (In reality, this condition is reached asymptotically as $GJ \to \infty$.) Eventually, all the lines for $\rho' > 0$ converge to the same value of K_s (for a particular combination of ψ and θ that is), representing local buckling of the individual skin bays with clamped conditions at the stiffener locations. This is reflected by the "upper" horizontal lines that are visible in Fig. 3 for some combinations of ψ and θ, clearly picturing a bound for local buckling loads between the (almost) simply supported and fully clamped edge conditions at the stiffener locations.

The influence of the orthotropy parameters ψ and θ on the shear buckling behavior follows directly from Fig. 3. An increase of the θ parameter causes a substantial increase of the buckling load for all values of ψ. If $\psi < 1$, an increase of ψ (associated with a decrease in the number of buckling waves) causes the buckling load to decrease, whereas for $\psi > 1$ the reverse effect occurs. This is a direct result of ψ being a measure for the effective length of the local bay plates and is analogous to the phenomenon that for an isotropic plate the shear buckling load increases with the length and converges to the value for an infinitely long plate. The prominence of the effective length of the individual skin bays is additionally reflected by the fact that for the higher values of the ψ parameter and the flexural stiffness parameter the difference in buckling loads between simply supported and clamped edges of the panel vanishes.

IV. Verification for Glare Panels

To assess the applicability of the presently discussed analysis procedure to the design of Glare shear panels, a number of more detailed FEM buckling analyses will be performed, again with the

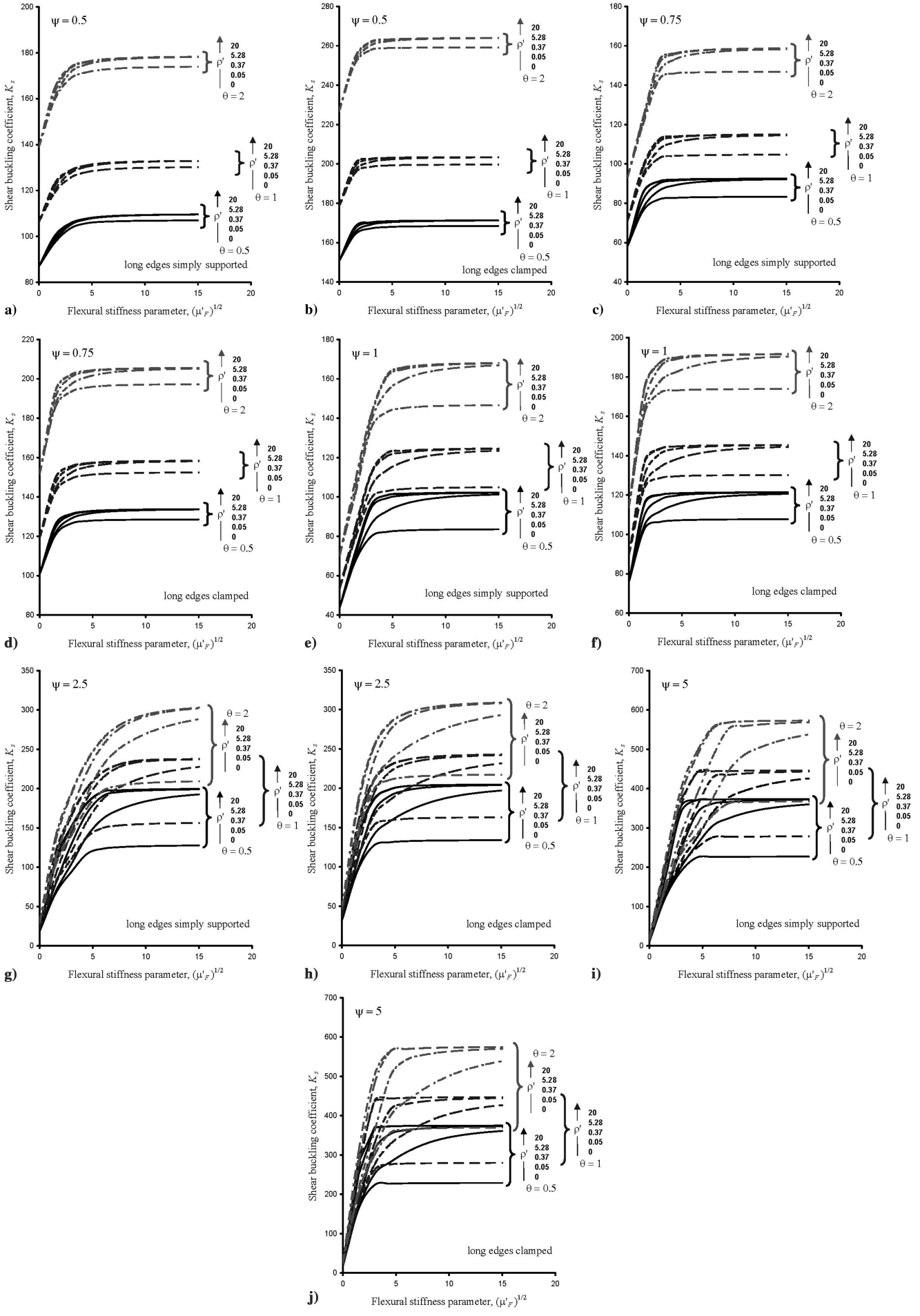

Fig. 3 Shear buckling coefficients for various values of nondimensional parameters for the long edges either simply supported or clamped.

Table 3 Configurations of Glare shear panels, with corresponding values of nondimensional design parameters, which are used to verify the design curves. The buckling loads are plotted in Fig. 5

Panel no.	1	2	3	4	5	6	7	8
Glare 3 conf.	5/4-0.4	3/2-0.3	5/4-0.4	3/2-0.3	5/4-0.4	3/2-0.3	5/4-0.4	3/2-0.3
Cross section	Open	Open	Open	Open	Closed	Closed	Closed	Closed
Attachment	Riveted	Riveted	Bonded	Bonded	Riveted	Riveted	Bonded	Bonded
t, mm	3.016	1.408	3.016	1.408	3.016	1.408	3.016	1.408
ψ	4.96	4.93	4.96	4.93	4.96	4.93	4.96	4.93
θ	0.91	0.94	0.91	0.94	0.91	0.94	0.91	0.94
$(\mu'_F)^{1/2}$	2.90	5.48	2.90	5.48	2.83	5.40	2.83	5.40
ρ'	0.14	0.15	0.14	0.15	9.24	10.21	9.24	10.21
K_s	227.8	400.8	202.7	383.9	318.5	431.2	327.7	429.0

STAGS code. The increased detail lies in the fact that the exact shape of the stiffeners is modeled this time (with 410-type shell elements). In this way, a number of realistic phenomena, such as the local deformation of the individual stiffener segments, the distortion of the stiffener cross section, eccentricity effects, and interaction between the stiffener and skin deformations can be accounted for. Also, the effect of the stiffener-skin connection (riveted or bonded) can be studied by using these more detailed models.

Glare is built up from alternate aluminum and glass fiber preimpregnated layers. The most common type of aluminum applied in Glare is 2024-T3 alloy. Each glass prepreg layer is composed of a certain number of unidirectional (UD) plies, which are stacked either unidirectionally or, most commonly, in a cross-ply arrangement. The number, orientations, and stacking sequence of the UD plies in the prepreg layers depend on the Glare *grade*. For example, a Glare 3 has two UD plies in a cross-ply arrangement (0/90 deg) in each glass layer, while in Glare 4 the prepreg layers consists of three UD plies stacked at 0/90/0 deg. Note that the outer layers in Glare are always aluminum, so that the number of glass fiber layers is always one less. A general Glare configuration is represented as

$$\text{Glare } grade - N_{\text{al}}/N_{\text{gl}} - t_{\text{al}}$$

where

grade = a number indicating the Glare grade (currently 1, 2, 3, 4, and 5);

N_{al} = number of aluminum layers;

N_{gl} = number of glass fiber layers, $N_{\text{gl}} = N_{\text{al}} - 1$;

t_{al} = thickness of the aluminum layers.

For example, Fig. 4 shows a typical Glare 3-3/2 laminate. It should be noted that the standard Glare types were derived for applications in fuselage structures, and therefore the fibers are aligned with the stringers and frames. (For a full, in-depth description of the Glare material and its applications to airframe structural design the reader is referred to [16].)

In the present investigation two types of stiffeners are considered: the first one has an open cross section (Z shaped), the second type a closed cross section (rectangular tube). The intention here is to analyze a low and a high value of μ'_F for both stiffener shapes (to capture different buckling modes), using both riveted and bonded connections, for a panel geometry with $a/b = 5$ (which is selected rather arbitrarily, but is yet representative for a "large aircraft" type of fuselage structures) and a total number of 10 stiffeners (simulating infinite width). The different values of μ'_F are obtained by varying the stiffener properties (such as the thickness, the width of the flanges, and the height), the stiffener pitch, and the skin thickness. The latter is actually done by using two different Glare types, being Glare 3-5/4-0.4 ($t = 3.016$ mm) and Glare 3-3/2-0.3 ($t = 1.408$ mm). A Glare 3 panel has an equal amount of glass fibers in the directions parallel and perpendicular to the stiffeners and satisfies the conditions of special orthotropy. The skin-stiffener connection in the FEM model is established through rigid links; for the riveted panels, these links are created along the center line of the stiffener flange and the corresponding nodes of the underlying skin; for the bonded connection, all overlapping nodes of the stiffener lower flange and the skin are rigidly linked together. The panel configurations with corresponding values of the design parameters ψ, θ, μ'_F, and ρ', and the calculated nondimensional buckling loads of the panels analyzed are presented in Table 3. The results of the detailed FEM analyses are also plotted in Fig. 5 together with design curves obtained from the calculation procedure discussed in Sec. II.B.

In the determination of the stiffener flexural rigidity EI, the second moment I was calculated for the combination of a single, central stiffener and a piece of skin of width b with respect to their combined neutral axis. For the riveted panels, the width of a skin bay was taken as the distance between the rivet lines; for the bonded panels, this quantity was taken as the stiffener pitch of the panel minus the width of the stiffener flange attached to the skin. This means that in the calculation of the nondimensional panel parameters and the shear buckling coefficient from Eqs. (11–15), a value of $b-$ width of stiffener flange was used rather than b itself. This implies that, to obtain the same values of the panel parameters for the riveted and corresponding bonded panels, the stiffener pitch in the FEM models was increased for the bonded panels by the width of the stiffener flange. For example, the stiffener spacing of panel 1 is 100 mm and the width of the stringer flange attached to the skin is 20 mm; the

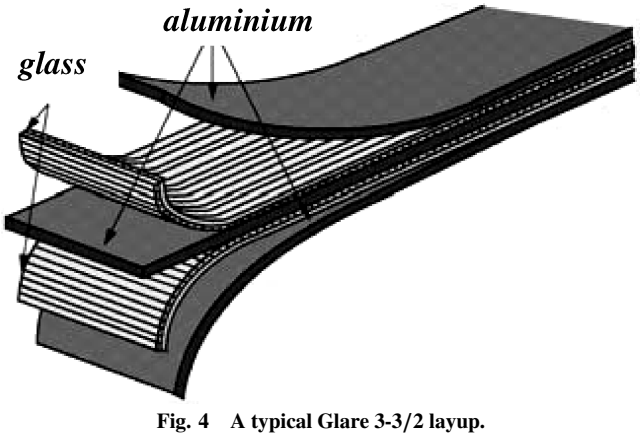

Fig. 4 A typical Glare 3-3/2 layup.

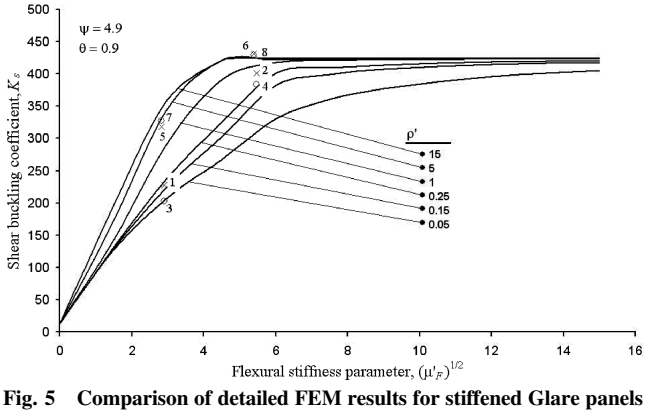

Fig. 5 Comparison of detailed FEM results for stiffened Glare panels with the calculation procedure discussed in Sec. II.B. (Numbers correspond to panel configurations in Table 3.)

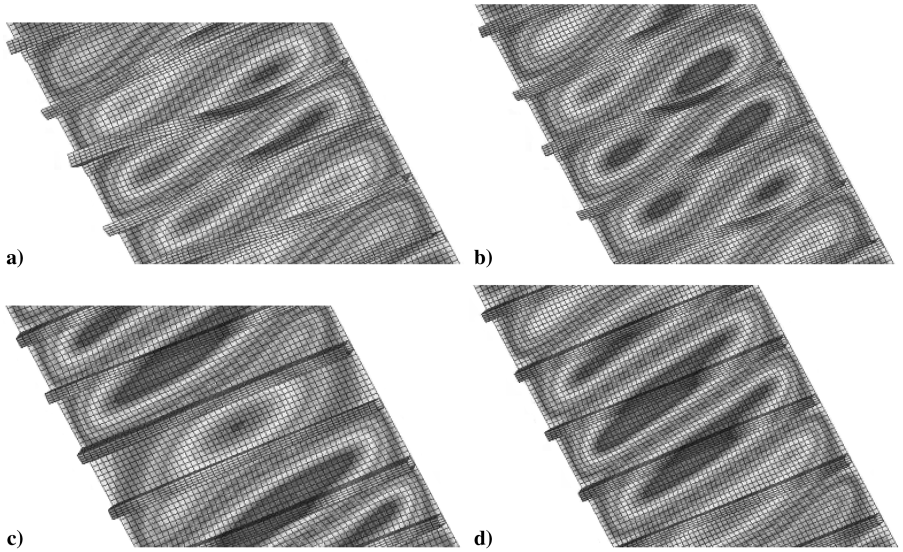

Fig. 6 Buckling modes of detailed FEM models for panels a) 1; b) 3; c) 5; and d) 7 as defined in Table 3.

stiffener pitch of the corresponding bonded panel 3, consequently, then is equal to 120 mm.

Examination of Fig. 5 reveals that the design curves predict slightly unconservative results for panels 3, 5, and 7, but slightly overestimate the buckling loads for all the other panels investigated. This conservatism is seen to be highest for panels 2 and 4. The trend seems to be that the design curves are unconservative for lower values of the flexural stiffness parameter (overall buckling), but are conservative for higher ones (local buckling). The source of the unconservatism for the lower flexural stiffnesses may be sought in interaction effects between the stiffeners and the skin, such as was caused by (local) distortion of the cross sections/rolling of the stiffeners, and/or the eccentric position of the stiffeners with respect to the skin, which are not accounted for in the calculation of the design curves in Fig. 5. Overall it can be stated that the design curves agree reasonably well with the FEM results so that they may be conveniently used for design purposes.

Buckling modes of the panels in Table 3 with a low value of the flexural stiffness parameter are shown in Fig. 6. The open-section stiffeners (panels 1 and 3) show the tendency to distort/roll (interaction effect), whereas the closed-section stiffeners (panels 5 and 7) remain undistorted in the buckling process. The overall-type of buckling mode associated with the relatively low flexural stiffness of the stiffeners is clearly reflected by the "isolines" extending through the lines of stiffener locations.

V. Conclusion

In the present paper the shear buckling behavior of flat, semi-infinite stiffened panels with a specially orthotropic skin plate was investigated. A total of four generic nondimensional panel parameters pertaining to the skin orthotropy and stiffener flexural and torsional rigidities were derived that, together with the boundary conditions at the long edges, fully describe the shear buckling behavior. A variety of design curves, relating the nondimensional shear buckling load to the four panel parameters, were calculated using a FEM-based procedure, in which beam elements were utilized to represent the stiffeners, and the validity of this procedure was demonstrated through comparison with an analytical solution. To assess the accuracy of the design curves in a realistic situation, a number of more detailed FEM analyses, in which the stiffener shape and attachment method were explicitly accounted for, were made for Glare panels with riveted or bonded, open or closed-section stiffeners. The results show that the design charts are reasonably accurate if the flexural rigidity of the stiffeners is calculated including the contribution of the skin plate over a width equal to the stiffener spacing, and with respect to their combined neutral axis.

References

[1] Kuhn, P., *Stresses in Aircraft and Shell Structures*, McGraw–Hill, New York, 1956.

[2] Stein, M., and Fralich, R. W., "Critical Shear Stress of Infinitely Long, Simply Supported Plate with Transverse Stiffeners," NACA TN-1851, April 1949.

[3] Cook, I. T., and Rockey, K. C., "Shear Buckling of Clamped and Simply-Supported Infinitely Long Plates Reinforced by Transverse Stiffeners," *Aeronautical Quarterly*, Vol. 13, No. 1, Feb. 1962, pp. 41–70.

[4] Cook, I. T., and Rockey, K. C., "Shear Buckling of Clamped and Simply-Supported Infinitely Long Plates Reinforced by Closed-Section Transverse Stiffeners," *Aeronautical Quarterly*, Vol. 13, No. 3, Aug. 1962, pp. 212–222.

[5] Rockey, K. C., and Cook, I. T., "Influence of the Torsional Rigidity of Transverse Stiffeners upon the Shear Buckling of Stiffened Plates," *Aeronautical Quarterly*, Vol. 16, No. 2, May 1964, pp. 88–131.

[6] Wittenberg, T. C., and Van Baten, T. J., "Exploratory Investigation of the Local-Overall Buckling Behaviour of Glare Shear Panels Including Plasticity Effects," *Proceedings of the 43rd AIAA/ASME/ASCE/AHS Structures, Structural Dynamics, and Materials Conference* [CD-ROM], AIAA, Reston, VA, 2002.

[7] Wittenberg, T. C., and Van Baten, T. J., "Shear Buckling Curves for Flat Stiffened Panels with Application to Glare Material," *Proceedings of the 44th AIAA/ASME/ASCE/AHS Structures, Structural Dynamics, and Materials Conference* [CD-ROM], AIAA, Reston, VA, 2003.

[8] Rankin, C. C., Brogan, F. A., Loden, W. A., and Cabiness, H. D., "STAGS Users Manual," Ver. 4.0, Lockheed Martin Missiles & Space Co., Inc., Palo Alto, CA, May 2001; also Report LMSC P032594.

[9] Bergmann, S., and Reissner, H., "Über die Knickung von Wellblechstreifen bei Schubbeanspruch," *Zeitschrift für Flugtechnik und Motorluftschifffahrt*, Vol. 20, No. 18, 1929, pp. 475–481 (in German).

[10] Seydel, E., "Wrinkling of Reinforced Plates Subjected to Shear Stresses," NACA TM-602, 1931.

[11] Seydel, E., "Ausbeul-Schublast rechteckiger Platten. (Zahlenbeispiele und Versuchsergebnisse)," *Zeitschrift für Flugtechnik und Motorluftschifffahrt*, Vol. 24, No. 3, 1933, pp. 78–83 (in German).

[12] Lekhnitskii, S. G., *Anisotropic Plates*, 2nd ed., Gordon and Breach, New York, 1968.

[13] Ashton, J. E., and Whitney, J. M., *Theory of Laminated Plates*, Technomic Publishing Co., Inc., Stamford, CT, 1970.

[14] Nemeth, M. P., "Buckling Behavior of Long Anisotropic Plates Subjected to Combined Loads," NASA TP-3568, Nov. 1995.

[15] Nemeth, M. P., "Buckling Behavior of Long Symmetrically Laminated Plates Subjected to Shear and Linearly Varying Axial Edge Loads," NASA TP-3659, July 1997.

[16] Vlot, A., and Gunnink, J. W. (eds.), *Fibre Metal Laminates: An Introduction*, Kluwer Academic, Dordrecht, The Netherlands, 2001.

B. Sankar
Associate Editor